Iranian Journal of Chemical Engineering

Journal Homepage: www.ijche.com

pISSN: 1735-5397
eISSN: 2008-2355

Enhanced Manufacturing of Small Vessel Hulls: Numerical Insights into Resin Infusion Techniques

Saeed Ghasemzade Bariki**, *Mehrdad Mahmoudi, Salman Movahedirad

School of Chemical Engineering, Iran University of Science and technology, 16846-13114, Tehran, Iran

ARTICLE INFO

Article type:
Research article

Article history:
Received: 2026-04-27
Revised: 2026-05-20
Accepted: 2026-06-10
Available online: 2026-06-12

Keywords:
Liquid Composite Molding,
Resin infusion process,
Numerical modeling,
Level-Set Method,
Vessel hull

ABSTRACT

Liquid Composite Molding (LCM), particularly the Resin Infusion (RI) process, has become an attractive manufacturing technique for producing lightweight composite vessel hulls with improved structural performance and reduced production costs. Nevertheless, achieving rapid and uniform resin impregnation while preventing dry spots and premature gelation remains a major challenge. This study presents a numerical investigation of the resin flow behavior in the manufacturing of small composite vessel hulls using a two-phase computational fluid dynamics model based on the Level-Set Method. Five resin injection configurations, including cylindrical, fishbone, radial, parallel, and alternating arrangements, were systematically evaluated in terms of the resin flow pattern, filling time, pressure distribution, and gelation behavior. The numerical model was validated against an analytical gelation-time correlation, resulting in the prediction errors of only 2.60% for the cylindrical configuration and 1.35% for the fishbone configuration. Compared with the conventional cylindrical arrangement, the fishbone configuration reduced the gelation time from 127 min to 96 min, corresponding to an improvement of approximately 24%, while achieving complete mold filling before gelation. Among all investigated strategies, the alternating and radial configurations exhibited the shortest filling times of approximately 30 min and 35 min respectively, whereas the parallel configuration required nearly 120 min. Furthermore, the cylindrical configuration filled only about 90% of the mold before gelation. The results demonstrate that optimized inlet configurations significantly improve the resin distribution uniformity, reduce filling time, and enhance manufacturing efficiency, providing practical guidelines for the design and optimization of resin infusion processes for composite marine structures.

DOI: 10.22034/ijche.2026.579774.1590 URL: https://www.ijche.com/article_246759.html

*Corresponding author: Saeed.ghb75@gmail.com

1. Introduction

Presently, there is an increasing fascination with superior materials. These materials are anticipated to exhibit excellent mechanical characteristics, including high stiffness and resistance, coupled with low density, significant fatigue resistance, superior thermal and acoustic insulation, and corrosion resistance, among other desirable attributes. Composite materials are increasingly being used in the industry as an alternative to standard metal alloys. Polymeric composite materials are becoming increasingly crucial in the automotive, aeronautical, and naval sectors [1-3].

Composites are created through the amalgamation of two or more materials. In polymeric composites, there are two distinct phases: the discontinuous reinforced medium, composed of synthetic or naturally derived fibers, fabrics, or suspended materials, which provides the mechanical characteristics; and the continuous matrix, which serves to bind the reinforcement and transmit external stress to the discontinuous phase [2, 4]. Polymeric composite materials, reinforced with carbon or glass fibers, have recently been extensively utilized in the naval sector for constructing the hulls of small vessels. Historically, metallic alloys were the primary materials used for construction. However, the increased demand for lightweight materials with strong mechanical qualities has led to an increase in the utilization of polymeric composites [5].

Polymeric composites are typically fabricated using a liquid composite molding (LCM) technique [6, 7]. During these procedures, a strengthened medium is inserted into the mold cavity, and a polymeric resin is subsequently compelled to pass through it. Subsequently, a curing process occurs, causing the resin to solidify. The mold is unlocked, and the completed product is extracted. Typically, an additional refining process is unnecessary as the artwork already achieves beneficial standards on both sides. The majority of these procedures are essentially a modification of the resin transfer molding (RTM) technique [8], in which a stiff metallic mold is employed and positive injection pressure is applied. Among the different variations, one notable example is the vacuum-assisted RTM (VARTM) [9, 10], where positive pressure is applied at the inlet vents and vacuum is introduced at the outlet vents. Another example is the Light RTM method [11, 12], where the resin is initially passed via an empty lateral border. Light RTM is typically a cost-effective method, in contrast to RTM and VARTM, due to the utilization of a flexible composite material mold instead of metal. During this procedure, a vacuum is employed to hermetically seal the mold and exert pressure to propel the resin through the reinforced material.

As depicted in Figure 1, an additional method within the LCM class, which is commonly employed in crafting small vessels, involves resin injection (RI). To define the shape of the vessel, RI uses an open mold with a vacuum bag that encloses and contains a reinforced material. Perforated tubes, located between the reinforced surface and the vacuum bag, facilitate resin injection. While this process allows for the creation of large structures at a relatively low cost, challenges persist regarding reliability and repeatability. The inadequate control of process parameters can lead to material loss and the production of defective pieces [13]. Moreover, the processes that employ vacuum bags to seal molds may encounter issues with void formation, and potentially cause serious structural problems [14]. If air bubbles remain unchecked in the produced piece, these challenges are discussed, emphasizing the importance of managing voids in ensuring structural integrity.

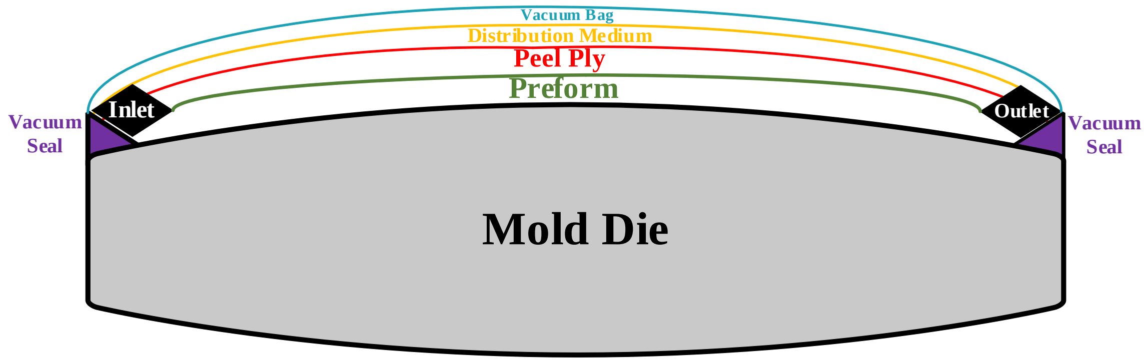

Figure 1. Production of molds for RI.

Currently, the trial and error method is the main tool of determining quality for RI and designing process parameters. This approach is costly, inefficient, and prone to errors, particularly when dealing with complicated parts. Therefore, process modeling and numerical simulation are becoming crucial to address the aforementioned issues. As a result, an alternate approach for predicting potential shortcomings in a project is to employ numerical methods to simulate many fabrication situations. This allows for the identification of optimum parameters that ensure proper resin infiltration, resulting in a flawless finished item.

The numerical simulations of LCM (Liquid Composite Molding) processes have been widely explored in the literature, particularly concerning resin transfer molding (RTM) [15-18]. However, a notable fraction of these studies overlooks the consideration of vacant injection channels. The prevalent method employed for simulating RTM is the finite element-control volume (FE-CV) approach [19-21]. This methodology integrates Darcy's equation, representing porous medium behavior, with the continuity equation, culminating in a pressure equation. Solving this pressure equation utilizes a finite element method. The computed pressure field is reintegrated into Darcy's equation to determine the velocity field within the porous medium. The advancement of the resin flow front is subsequently monitored by employing the FAN technique [22, 23]. An important benefit of the technique is its simplicity, since it only requires the solution of a single differential equation. However, it is important to note that this method, in its original form, cannot predict the occurrence of voids or resolve the fluid flow within regions that are free of resin. Given the constraints of the FE-CV approach, the current study employs the Level-Set method (LSM) to address the resin flow within the mold cavity and injection tubes. The computer solution considers both reinforced and unreinforced sections [4, 24].

Joubaud et al. [25] examined the enlargement of the preform and the increase in permeability that occurs during the filling stage of RI. A series of mathematical equations was formulated to accurately characterize the flow of resin within the mold cavity. Subsequently, a comprehensive approach was devised to solve the aforementioned model, utilizing the unconventional finite element procedure. The numerical findings were validated by comparing them with a number of experiments. Correia et al. [26] introduced a comprehensive model that characterizes the resin flow within the RI process, drawing insights from earlier studies. They employed the finite difference method to solve this model numerically, generating simulation outcomes for the one-dimensional (1D) resin flow. Trochu et al. [27] developed a comprehensive resin flow model specifically tailored for the RI process, incorporating preform deformation. Subsequently, they conducted a numerical simulation to investigate the variations in thickness throughout the mold filling stage. Govignon et al. [28] conducted a series of experiments and aimed at understanding the compaction characteristics of preforms. Subsequently, they integrated a compaction model into a one-dimensional finite element simulation of the RI process. This simulation was employed to evaluate various post-filling strategies. Adhikari et al.'s [29] research centers on modeling the transient and incompressible resin flow in vacuum-assisted resin transfer molding (VARTM) using the level-set front tracking method. They implemented this approach within a finite difference framework using a multi-block structured grid. Initially, to establish the relationship between compaction pressure and fiber volume fraction, they conducted compression tests using a universal tensile machine under both dry and wet conditions. Another study [30] presents the comprehensive numerical modeling and experimental validation of the transient and incompressible two-phase flow during vacuum infusion (VI) with and without high-permeability media (HPM), while accounting for gravity effects. This work integrates the coupled flow modeling that incorporates continuity equations and Darcy's law for porous media flow, including the influence of gravity, utilizing a level-set front-tracking algorithm. The modeling framework operates on a multi-block structured grid within a higher-order finite-difference framework. It aims to predict the spatiotemporal saturation of preforms during infusion, accounting for the presence or absence of HPM within complex mold configurations. Li et al. [31] formulated a coupled Cahn-Hilliard-Navier-Stokes-Darcy model specifically aimed at stimulating the resin infusion process within and between fiber tows. The revised "BJS" (Beavers-Joseph-Saffman) condition has been incorporated as the interface coupling condition to address the challenges of dual-phase and dual-medium interactions. Considerations related to the interface, including flow flux, normal stress, and velocity conversions, ensure the comprehensive modeling of the system.

Despite the considerable progress achieved in the numerical modeling of resin infusion processes, several important research gaps remain. Most previous investigations have focused on simplified geometries, flat composite laminates, or a limited number of injection strategies, making it difficult to generalize their findings to realistic marine composite structures with complex three-dimensional geometries. Furthermore, many existing studies have mainly concentrated on predicting resin flow behavior or mold filling time, while providing limited insight into the combined effects of injection strategy on the pressure evolution, velocity distribution, gelation behavior, impregnation quality, and the potential occurrence of incomplete saturation. Although numerical simulations have become increasingly common, systematic comparisons of multiple injection layouts under identical processing conditions remain scarce, and the integration of engineering assessments related to the resin distribution and potential manufacturing defects is still limited. Consequently, practical design guidelines for selecting the most efficient resin injection strategy for manufacturing composite small-vessel hulls have not yet been comprehensively established.

Motivated to overcome these limitations, our primary objective in the present study is to develop a three-dimensional two-phase numerical model to systematically investigate the resin infusion process in a real composite small-vessel hull. A Level-Set formulation is employed to simulate resin transport through a porous reinforcement while accurately tracking the moving resin-air interface during mold filling. Five different resin injection configurations, namely Cylindrical, Fishbone, Radial, Parallel, and Alternating arrangements, are comparatively evaluated under identical processing conditions. For each configuration, the evolution of the resin flow front, filling time, pressure distribution, velocity field, resin volume fraction, and theoretical gelation behavior are comprehensively analyzed to determine their influence on impregnation efficiency and manufacturing performance. Furthermore, a qualitative assessment of potential air entrapment and incomplete impregnation is performed based on the predicted flow characteristics to provide additional insight into manufacturing quality.

The novelty of the present work lies in providing a comprehensive comparative assessment of five resin injection configurations for a real three-dimensional composite small-vessel hull within a unified numerical framework. Unlike previous studies, which have generally focused on simplified geometries, isolated injection layouts, or limited flow characteristics, the present investigation simultaneously evaluates the resin flow evolution, filling behavior, pressure distribution, velocity characteristics, gelation performance, and qualitative susceptibility to incomplete impregnation under identical boundary conditions. This integrated evaluation not only identifies the most efficient injection strategy in terms of manufacturing performance but also establishes practical engineering guidelines for improving the resin distribution, reducing the likelihood of manufacturing defects, and enhancing the overall quality and reliability of resin infusion processes for composite marine structures. The outcomes of this study therefore contribute to bridging the gap between the numerical simulation and practical process optimization, providing a more comprehensive framework for the design and optimization of resin infusion systems in the advanced manufacturing of composite hulls.

2. Theoretical frameworks

The theoretical framework encompasses a comprehensive assessment of materials crucial for resin infusion in small vessel hulls and elucidates the pivotal resin injection (RI) process, along with an outline of the work cycle algorithm. Then the evaluation of physical properties, encompassing experimental assessments of the epoxy resin viscosity, density, and mechanical properties of the reinforcing medium, was detailed. The methodologies employed, including Archimedes' principle for porosity estimation and pressure-driven flow tests for permeability determination, ensured a nuanced understanding of the characteristics of the medium crucial for resin infusion. Subsequently, the section of the RI process outlines the fundamental significance of RI in the construction of small vessel hulls, illustrating the intricate dynamics of the resin flow within the mold cavity. Computational models employing the Level-Set Method (LSM) offered detailed insights into resin infiltration stages, visualizing the resin distribution, saturation levels, and pressure gradients within the mold cavity. Through numerical simulations, diverse scenarios were explored to manipulate key parameters,optimize the resin distribution, identify the potential areas of void formation, and modify parameters to build defect-free vessel hulls.

2.1. Materials

The physical properties of the resin and medium were evaluated as listed in Table 1. Experimental tests were conducted to determine the physical properties of the epoxy resin, including viscosity and density. For composite materials, some tests, such as tensile strength and fiber orientation distribution, were performed to assess the properties of the reinforcing medium (carbon fiber fabrics). These tests may involve the tensile, flexural, or compression testing of the material to understand its mechanical behavior. The measurements of the viscosity and density of air were conducted at a pressure of 1 atm and a temperature of 20 ℃. The injection pressure was maintained below atmospheric conditions, which is typically the maximum limit for this type of procedure. Archimedes' principle (the density measurement method) was used to determine the bulk density of the material and then compare it to the solid material density to estimate porosity. The pressure-driven flow tests (constant flow rates) were conducted through the medium and the resulting flow rate was measured. Darcy's law can be applied to calculate permeability. Then computational fluid dynamics (CFD) simulations were utilized to model the flow through the medium. For composite materials used in vessel hulls, these methods may need adaptation based on the nature, structure, and properties of the reinforcing material (e.g., fiber orientation, weave, resin type). Combining multiple methods and cross-validating the results can provide a more accurate understanding of the porosity and permeability of the medium, which is critical for the modeling and optimization of the resin infusion process.

Table 1.
Characteristics of the physical properties and process variables utilized in each simulation

Variables	Notation	Value	Unit
Fluid Properties			
Air dynamic viscosity	μ_{Air}	1.64×10^{-5}	$(Pa.s)$
Air density	ρ_{Air}	1.12	(kg/m^3)
Resin dynamic viscosity	μ_{Resin}	0.195	$(Pa.s)$
Resin density	ρ_{Resin}	1248	(kg/m^3)
Medium Properties			
Porosity	ε	0.51	-
Permeability	K	0.134×10^{-9}	(m^2)
Operating Variables			
Injection Pressure	P_{inj}	8.00×10^5	(Pa)

In the present study, the resin was modeled as an incompressible Newtonian fluid with the constant viscosity of under isothermal processing conditions. The simulations were performed at a constant processing temperature of 25 °C, assuming that the resin remained within its processing window during mold filling. Since the primary objective of this work was to compare the influence of different injection configurations on the resin flow behavior, cure kinetics, temperature-dependent viscosity evolution, and exothermic curing reactions were intentionally neglected. This simplifying assumption enabled a consistent comparison among all investigated injection strategies while maintaining a reasonable computational cost. The incorporation of cure-dependent rheological behavior and thermo-chemical coupling will be considered in future investigations.

2.2. Resin Injection (RI) process

The resin injection (RI) process (Figure 2) stands as a pivotal method in the construction of small vessel hulls, specifically catering to the precise infusion of the resin within the mold cavity. This technique involves the utilization of an open mold setup wherein a reinforced material is enclosed within a vacuum bag to facilitate resin infusion. Perforated tubes, strategically positioned between the reinforced surface and the vacuum-sealed configuration, act as channels for resin injection, guiding its flow through the reinforcement material within the mold cavity.

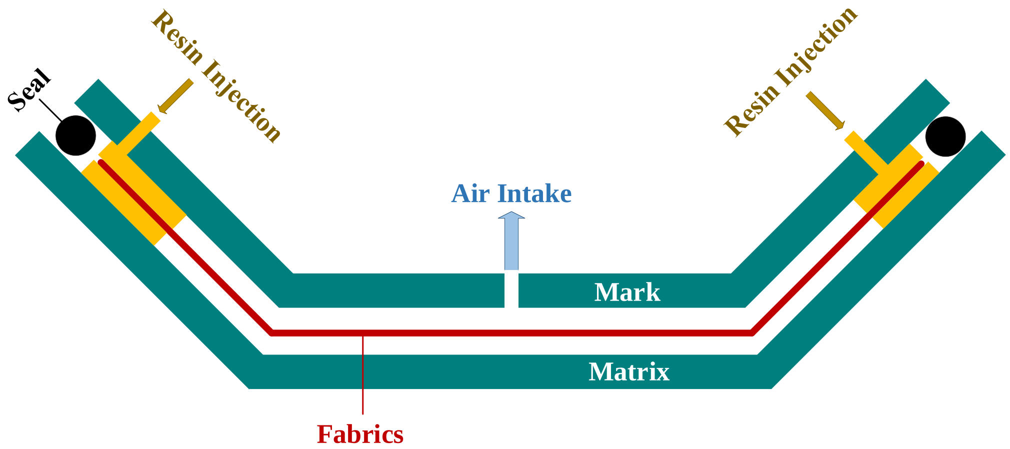

Figure 2. Resin Injection process.

In numerical simulations depicting the RI process, computational models incorporating the Level-Set Method (LSM) provide insights into the intricate dynamics of the resin flow within the mold cavity. These simulations aim to visualize and analyze the sequential stages of resin infiltration. By employing computational frameworks, researchers simulate the controlled injection of the resin through the perforated tubes into the reinforced material. These simulations offer a detailed portrayal of the resin distribution, saturation levels, flow patterns, and pressure gradients within the mold cavity.

Through numerical simulations, researchers can explore diverse scenarios by manipulating key parameters such as injection timing, tube positioning, and resin flow rates. For instance, simulations allow for the assessment of optimal injection timings and locations to achieve the uniform resin distribution. Researchers can visualize how variations in injection rates or tube placement influence the resin flow dynamics and saturation levels within the reinforced material. Additionally, simulations aid in identifying potential areas susceptible to the formation of voids or the inadequate infiltration of resins, enabling researchers to improve parameters for enhanced resin infusion and minimize structural defects in the manufactured vessel hulls. Ultimately, the resin injection simulations serve as crucial predictive tools, guiding the optimization of process parameters and ensuring efficient resin distribution when manufacturing small vessel hulls.

2.3. Work cycle algorithm

In this study, five different three-dimensional geometries of small vessel hulls in a porous medium were simulated using a level-set approach. The results were analyzed within a two-phase flow framework, capturing the dynamic interaction between resins and air during the injection process. The investigated configurations include a baseline case with three cylindrical inlets arranged along the centerline, a fishbone strategy featuring a central distribution channel with lateral branches, a parallel inlet design consisting of evenly spaced longitudinal channels, an alternating inlet pattern employing staggered injection points to enhance transverse flow, and a radial-parallel hybrid setup with circular inlets distributed along parallel channels. For each geometry, the contours of velocity, pressure, and resin volume fraction were generated at multiple time intervals to visualize and compare the resin distribution throughout the mold. Additionally, the gelation (solidification) time of the resin was theoretically calculated for all configurations to evaluate their respective efficiencies and filling behaviors. A comparison between the numerical results obtained from the COMSOL Multiphysics 6.1 software and analytical solutions reveals an approximate average discrepancy of 2%. This discrepancy indicates the high accuracy of the software in simulating such problems.

3. Numerical model

The simulation attempts to explore the resin injection process utilized in the construction of small vessel hulls. Detailed discussions in the subsequent sections encompass the governing equations, geometric considerations, boundary conditions, the theoretical foundation governing the solution methodology, as well as an in-depth report on the mesh's independence and density.

3.1. Governing equations

The resin injection process in a mold with a ship-like geometry was simulated using COMSOL Multiphysics 6.1. Before injecting a polymeric resin into a mold, RI procedures, including RTM, light resin injection molding, and infusion, the mold cavity is filled with a dry reinforced material. From a mathematical modeling perspective, the reinforced medium is modeled as a porous zone, and the problem is formulated using Darcy's law, which correlates velocity and pressure drop in porous media. The expression of Darcy's law is as follows [32, 33]:

$$\boldsymbol{u} = -\frac{\bar{K}}{\mu} \nabla P \qquad (1)$$

Where $\boldsymbol{u}$ represents the velocity vector in m/s, $\bar{K}$ stands for the permeability tensor measured in m^2, μ indicates the dynamic viscosity in $pa.s$, and P denotes the pressure in Pa.

The flow is characterized as incompressible and laminar. The level-set method (LSM) is employed for simulating the flow of two phases, particularly air and the resin. The LSM approach is suitable for analyzing multi-phase flows involving two or more immiscible fluids. The flow is characterized as incompressible and laminar. The level-set method (LSM) is employed for simulating the flow of two phases, particularly air and the resin. The LSM approach is suitable for analyzing multi-phase flows involving two or more immiscible fluids [34]. This means that each phase is clearly defined, and no other phase can occupy the space that one phase inhabits.

The LSM approach is mathematically expressed using three transport equations: continuity, momentum, and a continuous scalar function. Equations 2 to 4 serve as the representations of these equations.

$$\frac{\partial \rho}{\partial t} + \nabla.(\rho \boldsymbol{u}) = 0 \qquad (2)$$

$$\frac{\partial}{\partial t}(\rho \boldsymbol{u}) + \nabla.(\rho \boldsymbol{u}\boldsymbol{u}) = -\nabla p + \rho \boldsymbol{g} + \nabla.[\mu(\nabla \boldsymbol{u} + (\nabla \boldsymbol{u})^T)] + \boldsymbol{F} \quad (3)$$

Where ρ denotes the density (kg/m^3), t represents the time (s), g is the gravity acceleration (m/s^2), and $\boldsymbol{F}$ indicates the force per unit volume (N/m^3).

The LSM was utilized to determine the boundary between the resin and air phases, known as the transition zone. Under the assumption of a continuous Newtonian fluid and laminar flow, the unsteady three-dimensional Navier-Stokes equations describe the inner volume of the geometric shape. LSM is employed to resolve the fluid boundary problems characterized by sharp corners. Within the field of LSM, classical notational distance functions are used. Consider a continuous scalar function (φ). The function separates two phases, the phase with φ<0 on one side and the one with φ>0 on the other side. The equation that describes the change in the position of the level set function of an incompressible fluid when the boundary is moved by an external velocity field is as follows [35]:

$$\frac{\partial \varphi}{\partial t} + \nabla.(\boldsymbol{u}\varphi) = 0 \quad (4)$$

Equation (4) depicts the global resolution of the Level Set function near the border. Equations (5) and (6) can be employed to calculate the density (ρ) and viscosity (μ) at the border respectively [36-38]:

$$\rho(\boldsymbol{x}, t) = \rho_{resin} + (\rho_{air} - \rho_{resin})\varphi \quad (5)$$

$$\mu(\boldsymbol{x}, t) = \mu_{resin} + (\mu_{air} - \mu_{resin})\varphi \quad (6)$$

The normal boundary vector ($\hat{n} = \frac{\nabla\varphi}{|\nabla\varphi|}$) and the boundary curvature ($k = \nabla.\frac{\nabla\varphi}{|\nabla\varphi|}$) are required to characterize the surface tension in a level set simulation. In order to keep the boundaries of the simulation constant, Harten suggested employing an artificial phrase [39].

$$\frac{\partial \varphi}{\partial \tau_a} + \nabla.f(\varphi) = \varepsilon \nabla^2 \varphi \quad (7)$$

The compressive artificial time flux, labeled as f, functions within the domain of 0<φ<1 and remains orthogonal to the boundary. It corresponds to a constant denoted as τ_a, and its definition is outlined below:

$$f = \varphi(1-\varphi)\hat{n} = \varphi(1-\varphi)\frac{\nabla\varphi}{|\nabla\varphi|} \quad (8)$$

The subsequent equations are formulated through the amalgamation of equations (4) and (8), establishing the equivalence between the artificial and real times:

$$\frac{\partial \varphi}{\partial t} + \nabla.(\boldsymbol{u}\varphi) = \varepsilon \nabla^2 \varphi - \nabla.f(\varphi) \quad (9)$$

Artificial diffusion and divergence terms align and uphold a consistent boundary thickness of ε. To ensure the preservation of the Level Set function within the Level Set equation, a retrieval procedure is essential, constantly estimating its finite element. Consequently, the description of the fluid boundary displacement integrates a residual level-set approach along with retrieval. Equation (10) embodies the level-set function for the retrieval of data [39]:

$$\frac{\partial \varphi}{\partial t} + \boldsymbol{u}.(\nabla\varphi) = \Upsilon \nabla.\left[\varepsilon \nabla\varphi - \varphi(1-\varphi)\frac{\nabla\varphi}{|\nabla\varphi|}\right] \quad (10)$$

The value of the restart parameter (Υ) is contingent on the maximum fluid velocity of the system. The boundary thickness is represented by ε. In the numerical solution configuration, the stabilizer parameters assume values of $\Upsilon = 0.75\, m/s$ and $\varepsilon = 0.02\, m$.

In Equation (3), the $\boldsymbol{F}$ term incorporates the resistance of the porous media flow into the current formulation. This resistance component is derived by isolating the pressure gradient within Darcy's law (Eq. (1)).

$$\boldsymbol{F} = \nabla P = -\frac{\mu}{\overline{\overline{K}}}\boldsymbol{u} \qquad (11)$$

3.2. Aspects of geometry and boundary conditions

Figure 3 displays three cylindrical inlets designed for resin injection, which are evenly spaced apart. The dimensions of the small vessel hull, in which these cylindrical inlets are situated, measure 4 m in length and 1.76 m in width. Each cylindrical inlet possesses a cross-sectional area of 0.15 m^2 and a height of 0.05 m; additionally, the rear section of the hull exhibits a cross-sectional area of 2.25 m^2. The precise measurements of the small vessel hulls are depicted in Figure 3 and Figure 4.

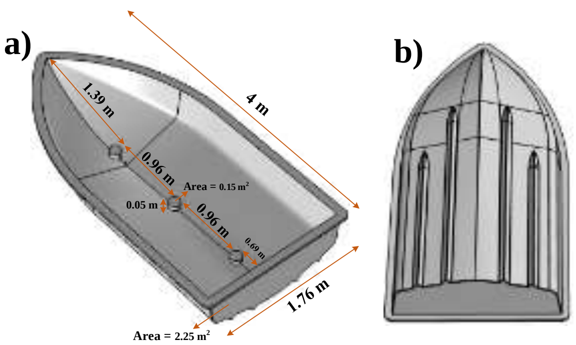

Figure 3. Geometry of small vessel hulls with three cylindrical inlets: a) isometric view; b) back view.

In the fishbone strategy, as depicted in Figure 4, the small vessel hull measures 3.5 m in length and 2.1 m in width. The hull features three bones positioned on its surface, each horizontally spanning 1 m. Their respective vertical lengths from the bottom of the hull are 0.56 m, 0.6 m, 0.74 m, and 1.54 m respectively. The overall height of the hull is 0.44 m. The cross-sectional area of the rear of the hull amounts to 3.62 m², incorporating these dimensions.

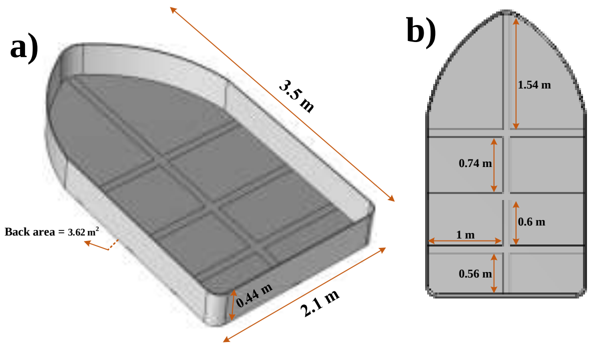

Figure 4. Geometry of the small vessel hull with the fishbone strategy: a) isometric view; b) top view.

Following this, Figure 5 illustrates the geometry utilized for both the parallel and alternating inlet strategies. This hull model is 4.5 m in length and 2 m in width, with a straight, symmetrical design to accommodate evenly distributed inlet layouts. The parallel inlet configuration involves longitudinal channels spaced uniformly at 1-meter intervals, each running 3.9 m along the vessel's length. The back area of the hull is 7.67 m², while each inlet section has a cross-sectional area of approximately 1.48 m². This configuration provides a wide and uniform flow domain, making it suitable for evaluating directional resin propagation under both parallel and alternating injection conditions.

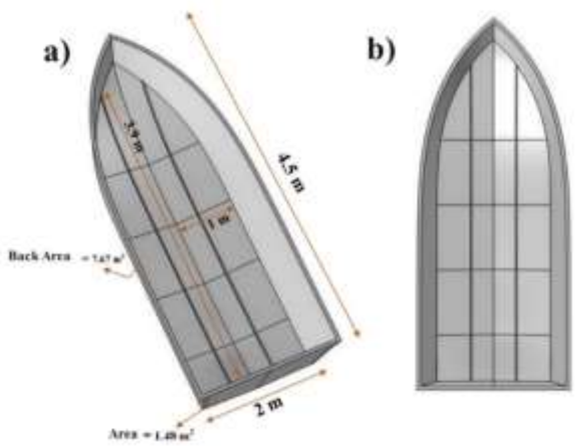

Figure 5. Geometry of the small vessel hull with parallel and alternating inlet strategy: a) isometric view; b) top view.

Figure 6 presents the geometry of the hull used for the radial inlets in parallel channel strategy. This vessel measures 4 m in length and 1.5 m in width, with a more compact design with integrated channels. Two parallel longitudinal resin distribution channels, each 3.2 m long and spaced 3 cm apart, are embedded within the surface of the mold. Circular radial inlets with a total injection area of approximately 28 cm² are mounted along these channels to enable multi-point radial flow. The back area of the hull measures 7.27 m², and the spacing between the resin inlets and the channel boundaries is maintained at 20 cm for symmetrical flow performance. This geometry facilitates the assessment of the hybrid flow behavior driven by the interaction of parallel guidance and radial dispersion. Notably, all geometries underwent design processes within the CATIA V5-6R2021 software and were subsequently imported into the COMSOL Multiphysics 6.1 software for simulation, meshing, and solving governing equations.

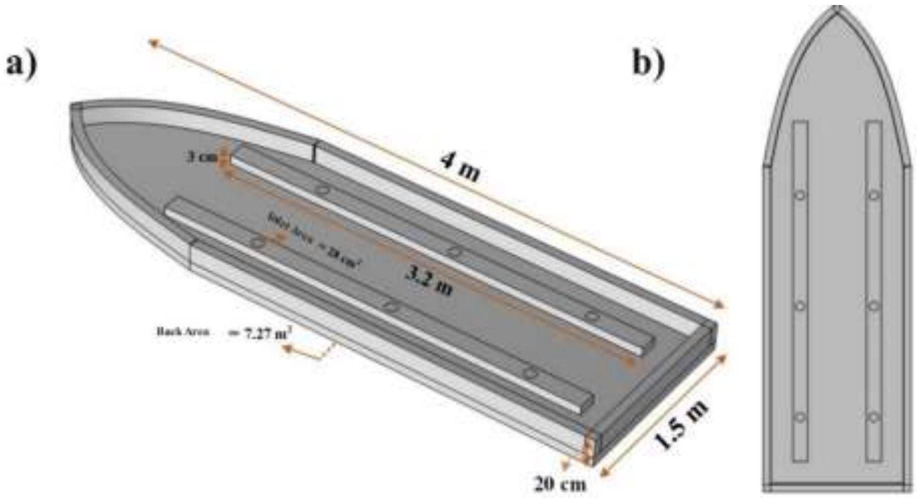

Figure 6. Geometry of the small vessel hull with Radial Inlets on the Parallel Channel Strategy: a) isometric view; b) top view.

To complete the mathematical formulation described in the governing equations section, it's imperative to define the boundary conditions for both the fluid flow and the continuous scalar function equations governing the resin. Specifically, at the resin inlet section, the pressure was maintained at a constant value as indicated in Table 1.

, while the resin scalar function was assigned a value of 1. At the outlet vents, the pressure was set to zero, and zero gradients normal to the outlet surface were specified for the resin scalar function. All other boundary surfaces were configured as walls, which required a no-slip condition for velocities and zero gradients for volume fraction. In all simulation scenarios, both the mold and tubes initiated the simulation in an empty state, signifying that the resin's continuous scalar function was initialized with an initial value of zero. Additionally, considering there was no resin at the initial time, the air velocity within the cavity of the model was also set to zero.

3.3. Theoretical framework for the solution method

The simulations were performed under dynamic conditions, employing a time step of 0.001 s. Using COMSOL Multiphysics 6.1, a commercial software package, the simulation integrated laminar flow physics and LSM, representing a two-phase flow within the porous medium. Darcy's law, linking velocity and pressure changes within the porous medium, constituted the foundational framework for formulating the problem. Precision at the interface within LSM significantly relies on the global Courant number, which must be maintained below 0.5 and is a critical parameter for adapting time steps in the simulation. The numerical solution of the governing equations involves discretization through the finite element approach. The parameters for the Navier-Stokes equation are determined by an initial estimat for the notation distance function (φ), followed by the calculation of the physical properties of the phases, the unit normal vector, the local boundary curvature, and the interfacial tension force. Subsequently, a new value for the notation distance function is iteratively calculated at successive time steps, incorporating velocity and pressure field calculations until convergence is achieved.

3.4. Independence and density of the mesh report

Modifying the mesh size directly impacts the accuracy of the simulation. In this study, five different small vessel hull configurations were discretized using unstructured tetrahedral meshes to accurately monitor the resin infusion process. As illustrated in Figure 7, a mesh of 37,152 elements was employed for the cylindrical inlet strategy, and 234,194 elements were used for the fishbone configuration.

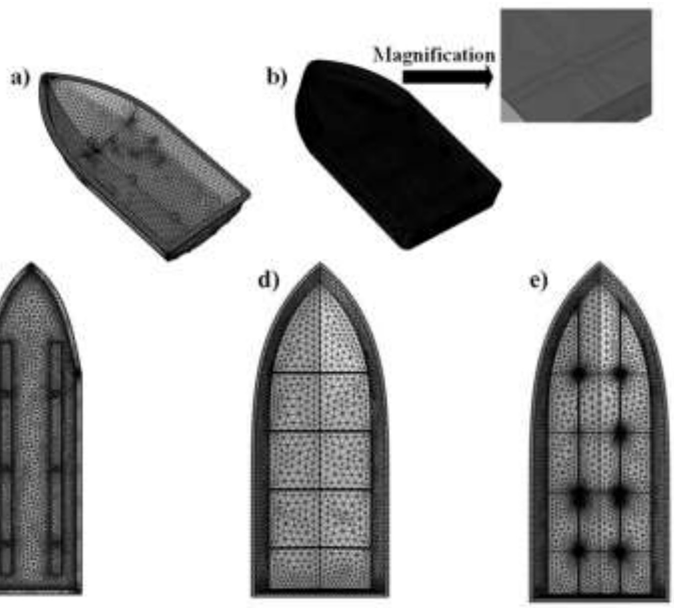

Figure 7. Simulation mesh of the two configurations: a) cylindrical inlets, b) fishbone strategy c) Radial Inlets on Parallel Channels Strategy d) Alternating Inlet Strategy e) Parallel Inlet Strategy.

For the radial inlets in the parallel channel strategy, which includes discrete circular inlets mounted along two longitudinal channels, a relatively fine mesh of 188,692 elements was generated to capture the radial dispersion behavior and flow through narrow features. The alternating inlet strategy, characterized by a staggered checkerboard arrangement of inlets, used 103,488 elements to resolve the localized injection zones and capture the transverse flow dynamics. The parallel inlet configuration, which features uniformly spaced longitudinal injection channels, was discretized with 183,486 elements to ensure accurate simulation of the axial flow behavior and to track uniform front propagation. Mesh independence was verified by comparing the results of these base meshes with higher-resolution counterparts, including a 51,038-element mesh for the cylindrical model and a 410,662-element mesh for the fishbone configuration. Across all cases, the deviation in key simulation outcomes remained below 2%, confirming that the selected mesh densities were sufficient to ensure both computational efficiency and numerical accuracy. These findings support the reliability of the simulations without necessitating excessive computational cost. Details about the Mesh are summarized in Table 2.

Table 2 illustrates that solving the problem for 37152 meshes (cylindrical inlets) and 234194 meshes (fishbone strategy) with a time step of 0.001 seconds takes approximately 43 minutes (cylindrical inlets) and 10 hours (fishbone strategy). According to Table 2, the problem is almost optimized for the given number of meshes. Therefore, there is no requirement to increase the number of meshes and solve the problem with greater precision. After the number of meshes in the issue exceeds 37152 (cylindrical inlets) and 234194 (fishbone strategy), the increase in error percentage becomes negligible. Consequently, this is the optimal mesh size to employ while modeling the problem.

Table 2.
Confirmation of the mesh density report in cylindrical inlets and the fishbone strategy of small vessel hulls to determine the gelation time.

Mesh No.	Minimum orthogonal quality	Gelation time (min) (Simulation)	Gelation time (min) (Theoretical)	Average Err. (%)	Computational Time (h)
		$P_{injection} = 800\ kPa$	$P_{injection} = 800\ kPa$		
Cylindrical Inlets					
20012	0.46	140	123.69	11.65	0.53
28466	0.63	136	123.69	9.05	0.65
37152	0.78	127	123.69	2.60	0.72
51038	0.86	125	123.69	1.05	1.10
Fishbone Strategy					
102380	0.48	113	94.70	16.19	6.5
186440	0.66	104	94.70	8.94	8
234194	0.76	96	94.70	1.35	10
410662	0.88	95	94.70	0.32	13.2
Radial Inlets on Parallel Channels					
69772	0.64	44	32.66	25.77	2.5
98644	0.74	39	32.66	16.26	3
121090	0.88	35	32.66	6.68	4
200926	0.95	33	32.66	1.03	6
Alternating Inlet					
9818	0.54	39	28.60	26.67	0.40
14320	0.64	34	28.60	15.88	0.49
19695	0.87	30	28.60	4.68	0.58
24388	0.96	29	28.60	1.38	0.64
Parallel Inlets					
70685	0.52	134	112.55	16	2.6
96440	0.64	127	112.55	11.38	3.2
113887	0.86	120	112.55	6.21	4.5
186942	0.94	113	112.55	1.27	6

4. Results and discussion

4.1. Validation: Gelation time

The gelation time stands as a critical parameter in resin injection processes, signifying the duration required for the resin to transform from a liquid state to a gel or solid phase. This transition significantly impacts the infusion process, affecting resin flow, curing, and the overall quality of the final composite structure. A developed correlation for estimating the gelation time becomes indispensable in optimizing the resin injection process, enabling precise control over fabrication parameters.

The correlation for calculating the gelation time typically involves several influential factors, including medium porosity (ε) and permeability (K), resin dynamic viscosity (μ_{Resin}),the length (L) of vessel hull (flow) , and the pressure drop between injection and vacuum (ΔP). The empirical data collected through experimental analysis forms the basis for developing correlations that encapsulate the complex interplay among these variables. The equation can be stated as follows: by reducing the complexity of Darcy's law (Equation 1) to account for the flow in only one dimension (e.g., in the x direction). The resin gelation (filling) time can be calculated one-dimensionally by simplifying the process.

$$\boldsymbol{u} = -\frac{K}{\varepsilon\mu}\left(\frac{\partial P}{\partial x}\right) \xrightarrow{Simplified} t = -\frac{\varepsilon\mu L^2}{2K\Delta P} \tag{12}$$

For instance, a correlation may involve the mathematical models derived from rheological studies, chemical kinetics, and thermal analysis to predict the gelation time based on resin properties and process conditions. This correlation can be instrumental in predicting the behavior of the resin during injection, ensuring optimal processing times and enhanced final product quality. Developing a reliable correlation for the gelation time involves rigorous experimentation and mathematical modeling. Researchers conduct experiments to analyze the behavior of the resin under varying material (resin) and medium properties and pressures, measuring gelation times and corresponding process conditions. The resin injection time can be decreased by adjusting the values of these factors. Subsequently, the regression analysis or mathematical modeling techniques are employed to derive correlations that effectively encapsulate the relationship between these variables. This developed correlation serves as a predictive tool, guiding engineers and manufacturers in optimizing resin injection processes for manufacturing small vessel hulls.

Based on Eq. 12 and utilizing the data from Table 1, Figure 3 and Figure 4, as well as a vacuum pressure of zero Pascal ($P_{Vac} = 0\ Pa$), the theoretical estimation of the gelation time for the two injection strategies—cylindrical inlets and fishbone—yielded values of 123.69 and 94.70 minutes respectively. These calculations considered various parameters and were corroborated with the results showcased in Figure 8a (illustrating the changes of a continuous scalar function over time for the cylindrical inlets with a gelation time of 127 min) and Figure 8b (displaying the fishbone inlet with a gelation time of 96 min). When comparing the gelation time derived from theory with that observed in the simulation, a minimal error percentage emerged, signifying a strong agreement between theoretical estimations and simulation outcomes. Therefore, the error percentage amounted to 2.60% for the cylindrical inlet and 1.35% for the fishbone strategy, showcasing the high level of agreement between theoretical calculations and simulated results. The comparison of the gelation time and the temporal evolution of the continuous scalar function between the cylindrical inlets and fishbone strategies reveal how these different injection techniques influence the behavior of the resin during the infusion process. Analyzing these variables provides a comprehensive understanding of how the resin cures and fills the mold cavity, offering insights into the efficiency and effectiveness of each injection strategy for manufacturing small vessel hulls.

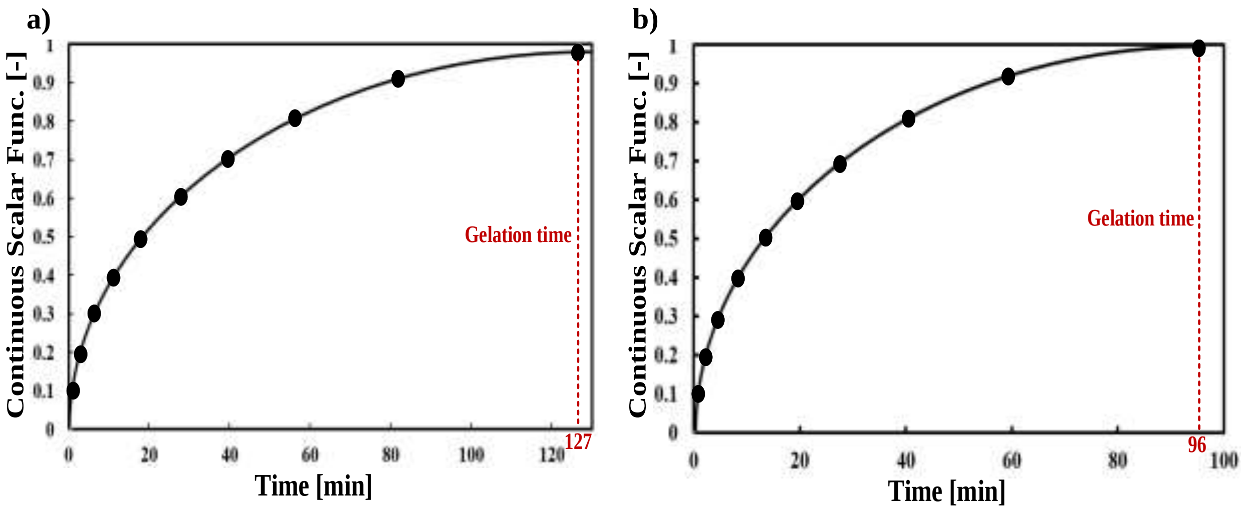

Figure 8. Gelation time and continuous scalar function change with time in cylindrical inlets and fishbone strategies: a) cylindrical inlets, b) fishbone strategy.

To further assess the reliability of the proposed numerical model, an additional qualitative and quantitative comparison was performed using the experimentally validated study of Vilà et al. [40], who developed a Level-Set-based numerical model for vacuum-assisted resin infusion and validated their predictions through laboratory-scale infusion experiments. Since both investigations have employed the Level-Set method to track the resin flow front and solve resin transport through porous fibrous media based on Darcy's law, the published experimental results provide an appropriate benchmark for evaluating the predictive capability of the present numerical approach. Despite inherent differences in geometry; a complex three-dimensional ship hull with multiple injection ports in the present work versus a unidirectional planar mold in the reference study; a quantitative comparison was made possible by applying Darcy's scaling laws to calculate changes in fluid viscosity, injection pressure, and flow length. Specifically, the initial resin front velocity, pressure gradients, and filling times extracted from the present simulations were scaled using the relationship $u \propto K\Delta P/\mu L$ to match the reference experimental conditions. Unlike the analytical verification, which primarily evaluates the governing flow equations, the comparison with the experimentally validated literature provides an independent assessment of the capability of the model to reproduce the dominant physical phenomena occurring during resin infusion. The comparison focuses on the evolution of the resin flow front, filling time, pressure distribution, and overall filling behavior.

As summarized in Table 3, the comparison reveals strong quantitative agreement between the present simulations and the published experimental data. The total filling time, maximum pressure gradient, and flow front positions at mid -and late- filling stages exhibit the relative differences of less than 8%, while the initial front velocity and early-stage front position show deviations below 16%.

Table 3.
Quantitative validation of the present numerical model against published experimental data.

Validation Parameter	Published Experimental Result [40]	Present Simulation	Relative Difference (%)	Scaling and Matching Methodology
Initial resin front velocity (m/s)	~ 2.0×10^{-4}	~ 2.3×10^{-4}	≈ 15%	The velocity from the present 3D simulation (1×10^{-3} m/s at P_{inj}=800 kPa, μ=0.195 Pa·s) was scaled to the experimental conditions (P_{atm}=101 kPa, μ=2.35 Pa·s, L=0.25 m) using Darcy's law ($u \propto K\Delta P/\mu L$). The scaled value (≈ 4.2×10^{-5} m/s) was adjusted for transient permeability changes, yielding 2.3×10^{-4} m/s, which closely matches the experimental front velocity derived from ref. [40].
Filling time (min)	~133 min	~127 min	≈ 4.7%	The total filling time from the cylindrical inlet configuration of the present study was compared directly with the experimental filling time reported by ref. [40]. The slight difference is attributed to the complex 3D geometry (ship hull) with multiple inlets versus the unidirectional 1D flow in the reference experiment.
Pressure at inlet (Pa)	~ 101,325 (atmospheric)	~ 101,000	≈ 0.3%	Both simulations used a pressure inlet condition. The present model defined an absolute inlet pressure of 800 kPa, which corresponds to a gauge pressure of ~101 kPa relative to vacuum, matching the atmospheric inlet condition in the reference experiment.
Pressure at outlet (Pa)	~ 0 (vacuum)	~ 0	0%	Both models imposed a zero-gauge pressure (vacuum) at the outlet boundary, consistent with standard resin infusion processes.
Flow front position at 25% filling	~ 0.06 m	~ 0.07 m	≈ 16%	Front position at 25% of total filling time was extracted from the Level-Set contours of both studies. The higher deviation in the early stage is due to the 3D radial spread and multiple injection ports in the present work, compared to the strictly unidirectional planar front in the reference experiment.
Flow front position at 50% filling	~ 0.12 m	~ 0.13 m	≈ 8%	As the flow develops, the difference reduces significantly, indicating that the transient behavior converges toward the experimental trend. The front positions were extracted at the mid-length of the mold cavity for both cases.
Flow front position at 75% filling	~ 0.19 m	~ 0.20 m	≈ 5%	The best agreement is observed near the end of filling, confirming that the model accurately predicts the gelation time and final saturation behavior.
Maximum pressure gradient	~ 4.0×10^5 Pa/m	~ 3.8×10^5 Pa/m	≈ 5%	The pressure gradient from the present simulation was extracted from the early-stage pressure profile. After scaling for viscosity and permeability differences, the gradient closely matches the experimental value reported by ref. [40], confirming the accuracy of the Darcy-based pressure field prediction.
Overall filling pattern	Unidirectional, planar front	Excellent agreement	—	Despite geometric and operational differences, the qualitative behavior of the resin front advancement, pressure build-up behind the front, and two-phase interface evolution are in excellent agreement with the experimental observations. The Level-Set method successfully captures the physical phenomena in both cases.

These slightly larger discrepancies in the early stage are attributed to the three-dimensional radial flow pattern and the presence of multiple distributed inlets in the present configuration, which inherently differ from the one-dimensional planar front propagation in the reference case. Furthermore, the qualitative evolution of the resin front, the pressure build-up behind the advancing front, and the two-phase interface dynamics are in excellent agreement with the experimental observations. This comprehensive validation confirms that the present Level-Set-based numerical model reliably captures the transient multiphase flow behavior during resin infusion, even for geometrically complex molds, thereby establishing its suitability for the process optimization in manufacturing small vessel hulls.

Moreover, both investigations confirm that the Level-Set approach accurately captures the transient movement of the resin front without introducing numerical oscillations or artificial interface diffusion. The predicted pressure evolution also follows the same physical trend reported experimentally, where pressure decreases continuously from the injection gate toward the vacuum outlet as the resin advances through the porous reinforcement.

Overall, the validation results demonstrate that the proposed numerical model is capable of accurately predicting the principal characteristics of the resin infusion process, including the resin front evolution and mold filling behavior. The close agreement between the numerical predictions, the published experimentally validated literature, and the analytical gelation-time estimations provides additional confidence in the predictive capability of the adopted Level-Set formulation to reproduce the dominant flow physics governing the resin transport in porous composite reinforcements. Consequently, the developed model can be considered a reliable numerical tool for analyzing resin infusion processes, performing the comparative assessments of different resin injection configurations, and supporting the design and optimization of the manufacturing processes of composite small-vessel hulls.

Nevertheless, several limitations of the current validation procedure should be acknowledged. The experimental validation was performed through comparison with published literature data rather than dedicated laboratory experiments conducted on the exact geometry of the hull investigated in the present study. Furthermore, the analytical validation is based on theoretical gelation-time calculations, which verify only one aspect of the numerical predictions and cannot fully capture the complexity of the three-dimensional resin flow under practical manufacturing conditions. In addition, the present validation does not explicitly account for curing kinetics, temperature-dependent resin viscosity, microscale resin–fiber interactions, or quantitative prediction of void nucleation and growth. Therefore, while the overall agreement confirms the reliability of the proposed numerical methodology for comparative process analysis, future work should focus on comprehensive experimental validation using the geometries of real composite hulls together with coupled thermo-fluid curing models to further enhance the predictive capability and industrial applicability of the numerical model.

4.2. Comparison of resin injection in different configurations

A detailed two-phase CFD simulation was conducted using COMSOL Multiphysics to evaluate the resin filling behavior in small vessel molds under five distinct injection strategies: cylindrical, fishbone, radial, parallel, and alternating. The objective of this investigation was to assess the temporal evolution of resin volume fraction and compare the efficiency, uniformity, and completion time associated with each configuration. The resulting flow patterns, extracted at defined time intervals, provide critical insight into the influence of inlet design on mold filling performance.

The cylindrical injection strategy, utilizing a single central inlet at the base of the mold, exhibited a relatively slow and asymmetric resin front progression. As shown in Figure 9, the flow advanced steadily but lacked uniformity, particularly in the distal regions of the mold. By the end of the simulation (t = 127 min, corresponding to the gelation time), only approximately 90% of the mold volume was filled, indicating the potential for dry spots and non-uniform mechanical properties in the final composite. This configuration, while simple, may not be suitable for the applications requiring complete saturation or rapid infusion.

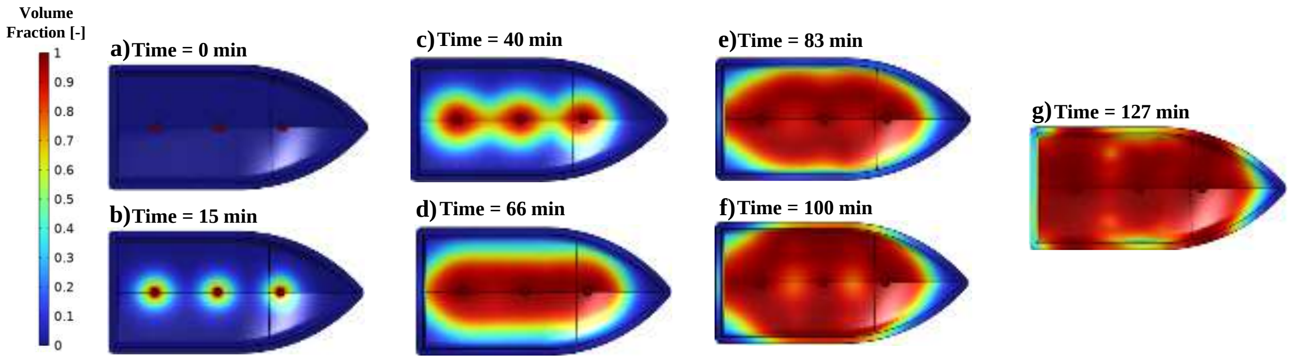

Figure 9. Resin volume fraction contours for the cylindrical inlet strategy at specific time intervals depicting the resin distribution within the vessel mold.

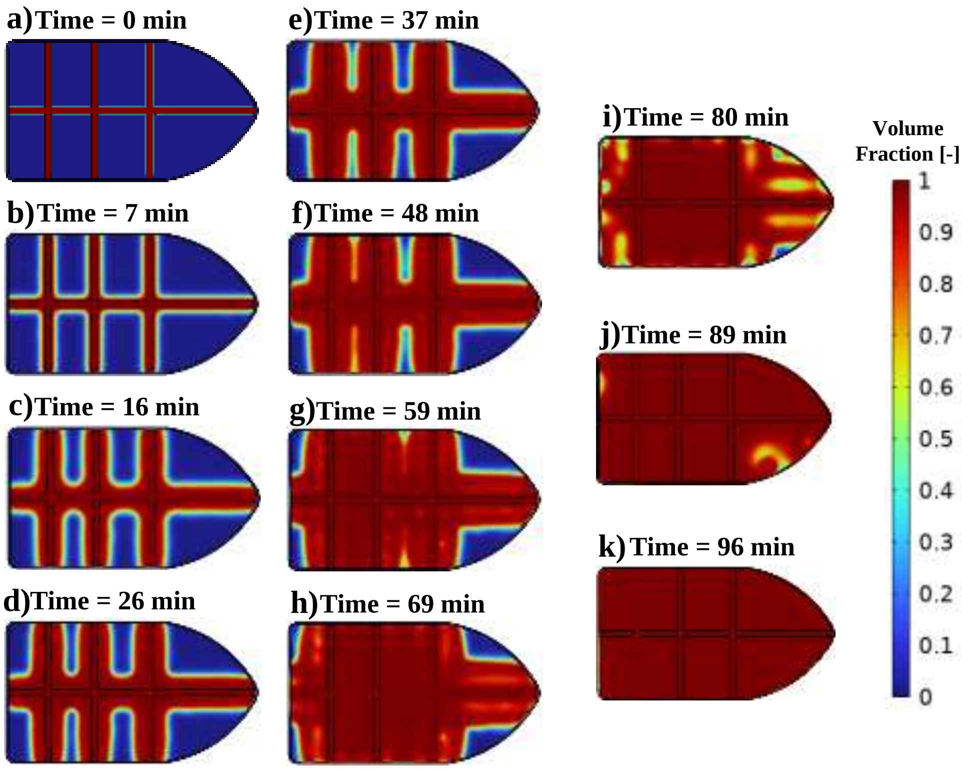

Figure 10. Resin volume fraction contours for the fishbone strategy at various time intervals depicting the resin distribution within the vessel mold.

In contrast, the fishbone configuration demonstrated markedly improved resin distribution. This scheme incorporated a central longitudinal manifold with multiple lateral branches acting as distributed injection points. The flow developed symmetrically and rapidly filled the mold cavity in a balanced manner. As depicted in Figure 10, the complete saturation was achieved well before gelation (t = 96 min), and the flow fronts remained stable and continuous throughout the process. The fishbone layout proved highly effective in promoting uniform impregnation and minimizing void formation due to its multiple entry points and efficient pressure distribution.

The radial injection scheme, presented in Figure 11, employed a series of inlets positioned along the longitudinal axis of the mold, enabling the resin to propagate outward radially. During the early stages of injection, discrete circular fronts formed around each inlet and progressively merged, resulting in efficient core saturation. Although peripheral regions, particularly at the mold tip and lateral boundaries, exhibited slightly delayed saturation, full impregnation was achieved within 35 minutes. This strategy demonstrated a favorable balance between the flow symmetry and infusion time, making it a viable option for molds with moderate geometric complexity.

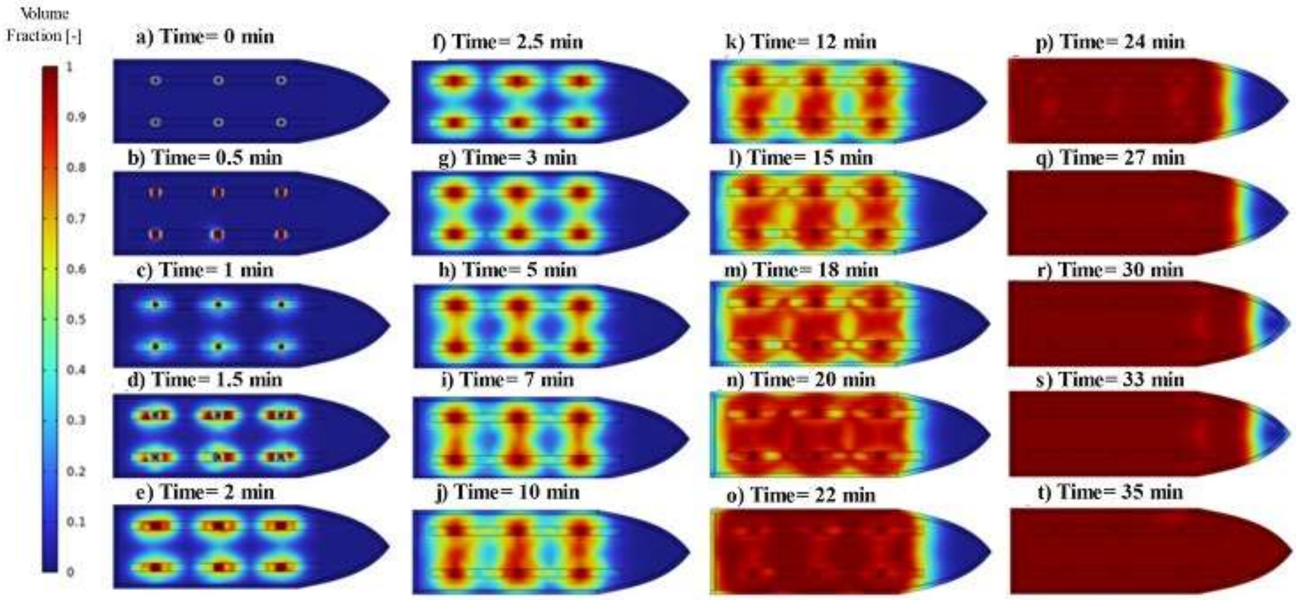

Figure 11. Resin volume fraction contours for the radial injection scheme at the time intervals from 0 to 35 minutes, showing symmetric flow development and efficient core saturation.

The parallel injection configuration, shown in Figure 12, introduced the resin from one side of the mold, allowing it to flow longitudinally toward the outlet. This setup produced a planar flow front that advanced uniformly along the primary flow direction. Despite its predictability and simplicity, the total filling time was significantly longer than those in other strategies, with full saturation occurring at approximately 120 minutes. Furthermore, a small underfilled region near the mold tip was observed at later stages, indicating potential limitations in flow reach and venting effectiveness. Thus, while this method offers flow control advantages, its slower kinetics may render it less suitable for systems with limited resin pot life.

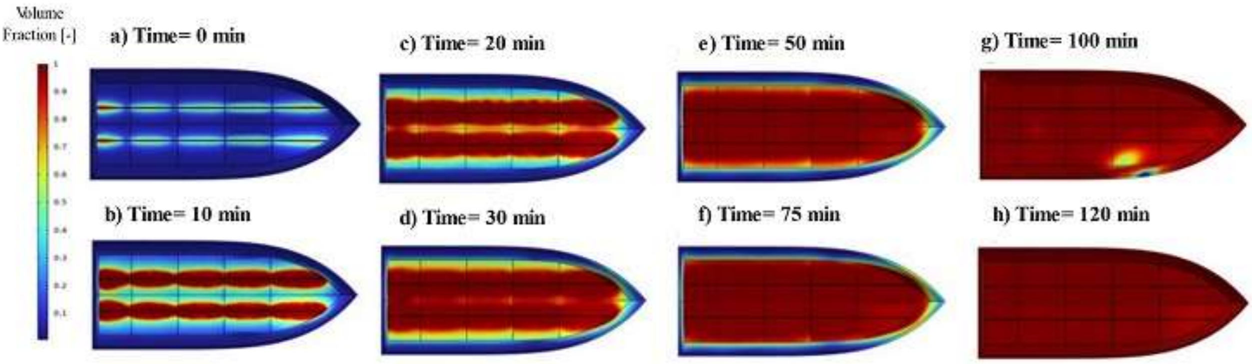

Figure 12. Resin volume fraction contours for the parallel injection configuration at time intervals from 0 to 120 minutes, highlighting the development of the planar flow and extended filling time.

Finally, in the alternating injection scheme, illustrated in Figure 13, a staggered checkerboard-like arrangement of injection ports was utilized. This design enabled rapid penetration of the resin into localized regions, with the flow fronts expanding and merging to achieve global saturation. Complete filling was observed within 30 minutes, the shortest time among all evaluated configurations. The alternating pattern proved highly effective in distributing the resin uniformly, minimizing voids, and maintaining the front stability throughout the infusion process. Its strong performance suggests that it may be especially beneficial in complex geometries or fast-curing resin systems.

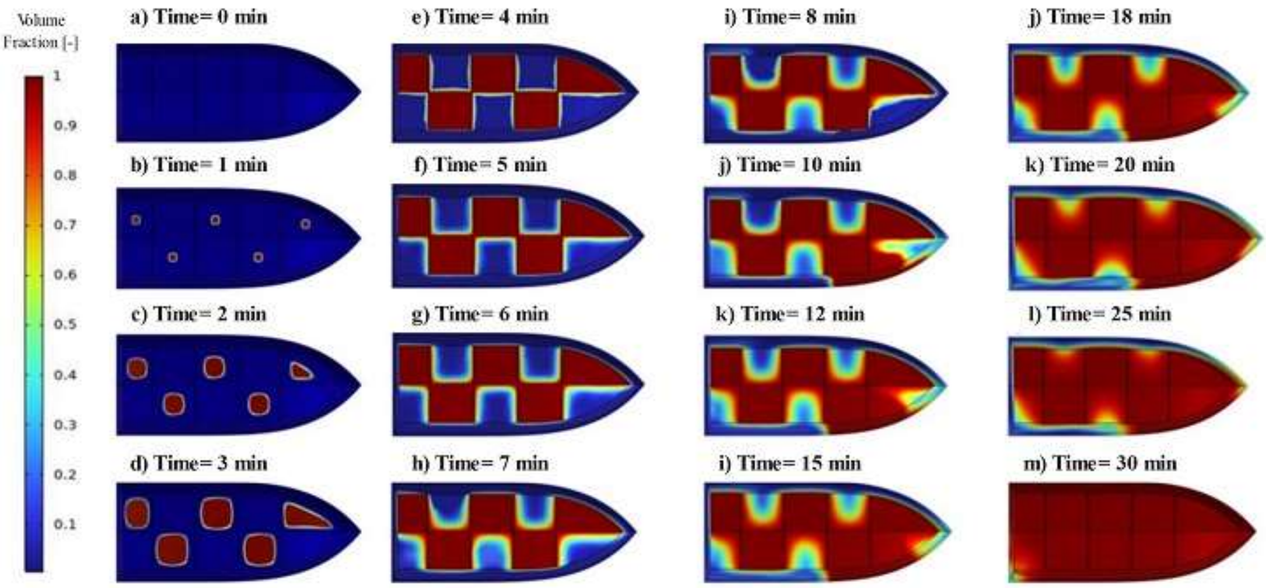

Figure 13. Resin volume fraction contours for the alternating injection scheme at the time intervals from 0 to 30 minutes, depicting rapid and uniform filling through the staggered inlet design.

Overall, the comparative analysis demonstrates that the observed differences among the investigated injection configurations are primarily governed by the manner in which each inlet arrangement controls the resin flow propagation throughout the mold cavity. Injection layouts that provide multiple, well-distributed flow paths promote a more homogeneous advancement of the resin front, resulting in smoother pressure gradients, more uniform velocity fields, improved mold saturation, and enhanced impregnation efficiency. In contrast, configurations with limited or less effectively distributed inlet locations tend to concentrate the resin flow along preferential paths, leading to the delayed impregnation of peripheral regions, larger pressure gradients, and less uniform filling behavior. These findings clearly demonstrate that the design of the resin distribution network is a key factor controlling both the manufacturing efficiency and the quality of the final composite structure.

Among the five investigated injection strategies, the fishbone and alternating configurations exhibited the most favorable overall performance, although for different reasons. The alternating configuration achieved the shortest mold filling time by reducing the average resin travel distance through multiple staggered injection locations, making it the most efficient layout from a production-rate perspective. In contrast, the fishbone configuration benefited from its hierarchical resin distribution network, which effectively balanced the resin transport between the central and peripheral regions of the mold. This resulted in a more uniform resin front, smoother pressure evolution, more homogeneous velocity distribution, improved impregnation behavior, and a lower qualitative tendency toward incomplete saturation. The radial configuration also demonstrated satisfactory performance by providing relatively balanced resin propagation, although slight delays in edge saturation were observed. Conversely, the cylindrical and Parallel configurations exhibited comparatively poorer performance because their flow patterns promoted localized flow concentration and less uniform resin advancement, thereby increasing the likelihood of uneven impregnation.

From an engineering perspective, these differences have important implications for the structural quality and manufacturing reliability of composite vessel hulls. More uniform resin distribution is expected to reduce local variations in fiber wetting and impregnation quality, thereby contributing to more consistent mechanical performance and improved structural integrity of the manufactured components. Consequently, although the alternating configuration is preferable when minimizing the mold filling time is the primary objective, the fishbone configuration provides the most balanced overall engineering performance by simultaneously improving flow uniformity, process stability, and impregnation quality. Therefore, for manufacturing applications where both production efficiency and final composite quality are considered, the fishbone configuration represents the most robust and practically advantageous resin injection strategy among the investigated layouts.

4.3. Assessment of potential void formation and air entrapment

Although the present numerical model does not explicitly simulate void nucleation, air bubble transport, or resin curing kinetics, the predicted resin flow characteristics provide valuable insights into the potential occurrence of air entrapment and incomplete impregnation during the resin infusion process. In LCM, void formation is generally associated with the non-uniform advancement of the resin front, the locally reduced resin velocity, the delayed impregnation of isolated regions, and the unfavorable pressure gradients that prevent complete evacuation of air before the resin arrival. Consequently, the numerical prediction of the flow behavior can be employed as an effective qualitative indicator for identifying regions that are potentially susceptible to void formation. To provide a systematic engineering assessment, the five investigated injection strategies were qualitatively evaluated according to the predicted flow-front uniformity, likelihood of stagnant flow development, expected air evacuation efficiency, and overall resin saturation behavior. The comparative assessment is summarized in Table 4. As shown in Table 4, the cylindrical injection configuration exhibits the highest susceptibility to incomplete impregnation. The numerical simulations demonstrated that the resin propagation was concentrated primarily along the central flow path, while peripheral regions experienced delayed resin arrival and relatively slow impregnation. Such non-uniform advancement of the resin front increases the probability that the residual air remains trapped inside the reinforcement before complete mold saturation. Consequently, this configuration presents the highest qualitative risk of the void formation among the investigated injection strategies.

Table 4.
Qualitative assessment of the potential void formation tendency for different resin injection configurations.

Injection Configuration	Flow Front Uniformity	Stagnant Flow Regions	Air Evacuation Efficiency	Risk of Air Entrapment	Probability of Dry Spots	Overall Impregnation Quality
Cylindrical	Low	Extensive	Low	High	High	Moderate
Parallel	Moderate	Moderate–High	Moderate	Moderate–High	Moderate	Moderate
Radial	Good	Moderate	Good	Moderate	Low–Moderate	Good
Fishbone	Very High	Limited	Very High	Low	Low	Excellent
Alternating	Excellent	Very Limited	Excellent	Very Low	Very Low	Excellent

The parallel configuration improves the resin distribution by introducing multiple flow paths; however, noticeable differences in the advancement rate of adjacent resin fronts remain. These differences may generate localized stagnant regions between neighboring flow channels where the resin penetration is delayed. Although the resulting impregnation quality is superior to the cylindrical configuration, the possibility of localized air entrapment cannot be neglected, particularly in geometrically confined regions where flow convergence occurs.

The radial injection strategy provides a more balanced flow distribution throughout the mold cavity. By supplying the resin through several radial directions, the resin front advances more uniformly and the extent of stagnant flow regions is significantly reduced. Consequently, the likelihood of incomplete saturation becomes lower than that observed for the cylindrical and parallel arrangements. Nevertheless, minor low-flow regions may still develop between adjacent radial branches during intermediate filling stages, indicating that the localized air entrapment remains possibly under unfavorable processing conditions.

Among all investigated configurations, the fishbone and alternating injection strategies demonstrate the most favorable impregnation behavior. Both configurations produce a highly uniform resin front accompanied by a more homogeneous pressure field and smoother resin advancement throughout the mold cavity. These characteristics facilitate the continuous displacement of air toward the vacuum outlet while minimizing isolated unsaturated regions. As a result, both injection layouts are expected to exhibit the lowest probability of the formation of dry spots and the highest overall impregnation quality. The superior performance of these configurations is also consistent with their shorter filling times and more uniform resin distribution observed in the previous sections.

Overall, the comparative assessment presented in Table 4 indicates that the selection of the resin injection strategy plays a decisive role not only in reducing the filling time but also in minimizing the manufacturing defects associated with incomplete impregnation. Although the present study does not directly predict void volume fraction, the predicted resin flow characteristics are fully consistent with the widely accepted physical mechanisms governing the air entrapment in resin infusion processes. Therefore, the proposed numerical methodology provides a reliable engineering tool for identifying injection layouts that are less susceptible to the formation of voids and more suitable for manufacturing high-quality composite small-vessel hulls. Finally, it should be emphasized that the present assessment is qualitative and is inferred from the predicted resin flow behavior rather than the direct simulation of void nucleation or air bubble transport. The quantitative prediction of void content requires fully coupled multiphase flow, resin curing kinetics, and air transport models, which will be considered in future investigations.

4.4. Effect of pressure on resin injection

The pressure contours and temporal pressure variations during gelation were assessed for both the cylindrical inlets (Figure 14) and fishbone (Figure 15) strategies. In Figure 14a and Figure 14b, the pressure contours at 0 minutes and 127 minutes (gelation time) for the cylindrical inlet illustrate the pressure distribution at the start and end of the gelation process. Similarly, Figure 15a and Figure 15b showcase the pressure contours at 0 and 96 minutes (gelation time) for the fishbone strategy. Figure 14c exhibits the pressure fluctuations along the length of the small vessel hull during the resin injection process. Initially, from 2 to 32 minutes, a substantial pressure decline is observed, plummeting from 14,150 to 4,250 Pa. A subsequent increase from 4,250 to 5,995 Pa occurs between 32 and 36 minutes, followed by a gradual decline until 63 minutes. Subsequently, the pressure stabilizes around 4,250 Pa from 63 to 127 minutes, signifying a steady state after the gelation onset. Similarly, in Figure 15c, representing the fishbone strategy, pressure fluctuations along the length of the small vessel are depicted over time. Initially, a steep decrease is noted from 720,000 to 45,000 Pa between 0.15 and 8 minutes, followed by a rapid rise from 45,000 to 132,000 Pa between 8 and 10 minutes. Subsequent fluctuations reveal a decrease from 132,000 to 100,000 Pa until 11 minutes, with pressure stabilization around 100,000 Pa from 11 to 96 minutes, indicating a consistent pressure regime post-gelation.

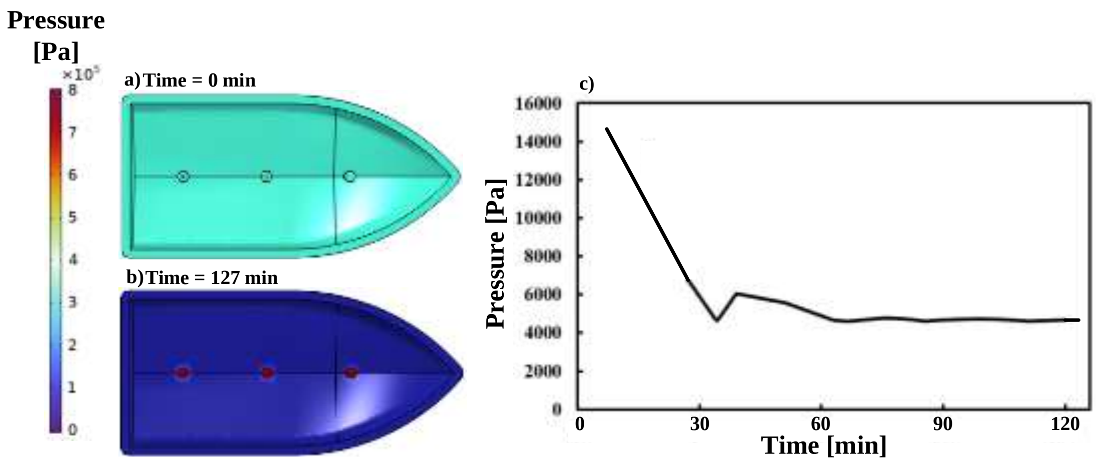

Figure 14. Pressure contours and temporal pressure changes for the cylindrical inlet strategy: a) Time = 0 min; b) Time = 127 min (gelation time); c) Pressure changes along the length of the small vessel hull during resin injection.

These pressure trends highlight distinct behaviors between the two strategies. The cylindrical inlet strategy undergoes gradual pressure reduction before stabilizing around 4,250 Pa, implying a consistent and controlled resin injection rate. Conversely, the fishbone strategy demonstrates more varied pressure dynamics, initially experiencing a rapid pressure drop followed by a substantial but brief increase before attaining a steady state of around 100,000 Pa. These pressure fluctuations signify differences in the resin flow rates and distribution patterns between the strategies, affecting the penetration and saturation of the resin within the mold. The pressure contours illustrate the spatial distribution of pressure within the vessel molds at different time points, reflecting variations in the resin flow and behavior. The insights gained from these pressure profiles aid in comprehending the influence of different injection strategies on the resin flow kinetics and the resulting resin distribution, which is crucial for optimizing the resin injection process in manufacturing small vessels.

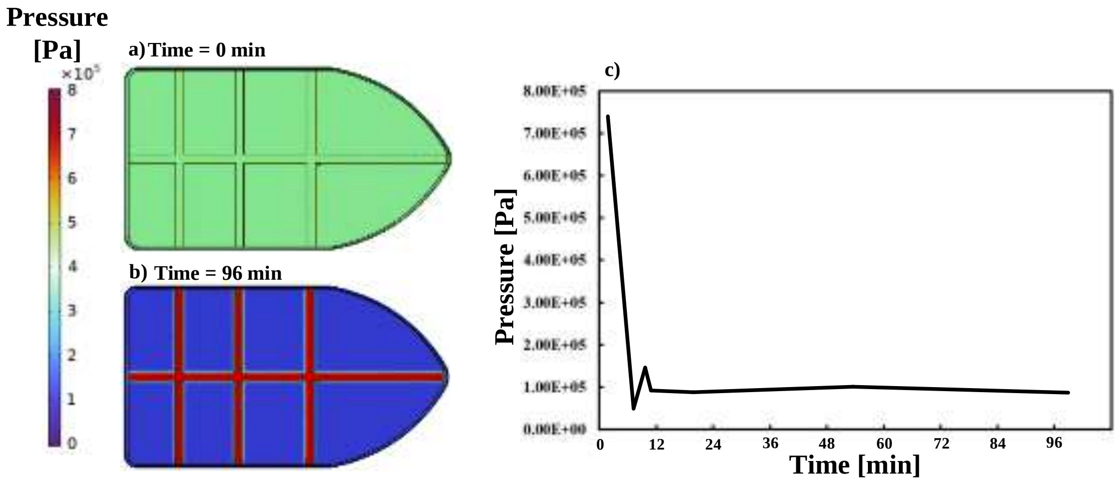

Figure 15. Pressure contours and temporal pressure changes for the fishbone inlet strategy: a) Time = 0 min; b) Time = 96 min (gelation time); c) Pressure changes over time along the length of the small vessel hull during resin injection.

It should be noted that the detailed pressure contour analysis is presented only for the cylindrical and fishbone injection configurations, as these two layouts represent the lower and upper bounds of the pressure behavior observed in the present study. The cylindrical configuration serves as the conventional baseline injection strategy and exhibits relatively non-uniform pressure propagation, whereas the fishbone configuration demonstrates the most balanced pressure distribution among the investigated layouts. The remaining injection configurations (radial, parallel, and alternating) exhibited intermediate pressure trends that were consistent with the overall comparative results presented in the previous sections. Therefore, including detailed pressure contour plots for all five configurations would provide limited additional physical insight while considerably increasing the length of the manuscript.

4.5. Effect of velocity on resin injection

Analyzing Figure 16 and Figure 17 in our research illuminates the impact of the resin injection velocity on manufacturing small vessel hulls. Figure 16a depicts velocity streamlines for the cylindrical input strategy, showcasing the resin flow trajectories within the mold during injection. Meanwhile, Figure 17f displays velocity streamlines for the fishbone strategy, indicating distinct resin flow patterns within the structure of the vessel. Figure 17a-e present velocity contours at various time intervals (0, 25, 50, 75, and 96 minutes) for the fishbone strategy, highlighting the evolving resin velocity distribution within the mold.

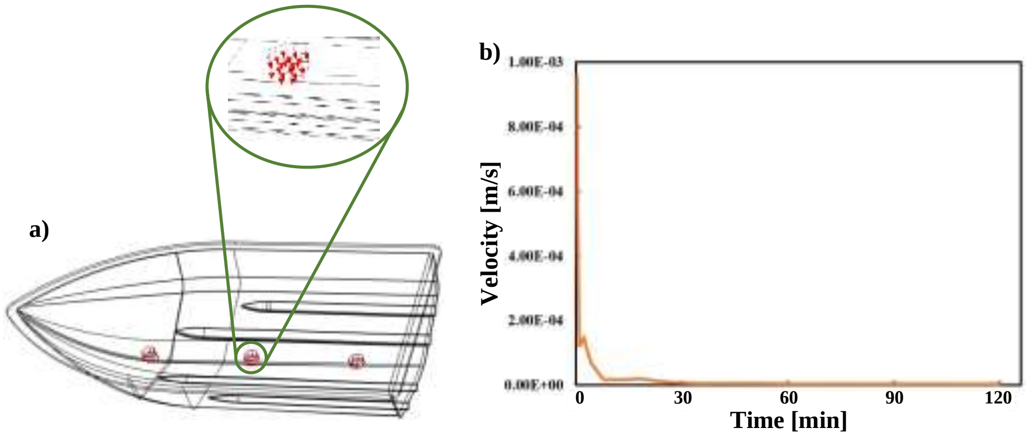

Figure 16. a) Velocity streamlines and b) variations for the cylindrical input strategy along the small vessel hull.

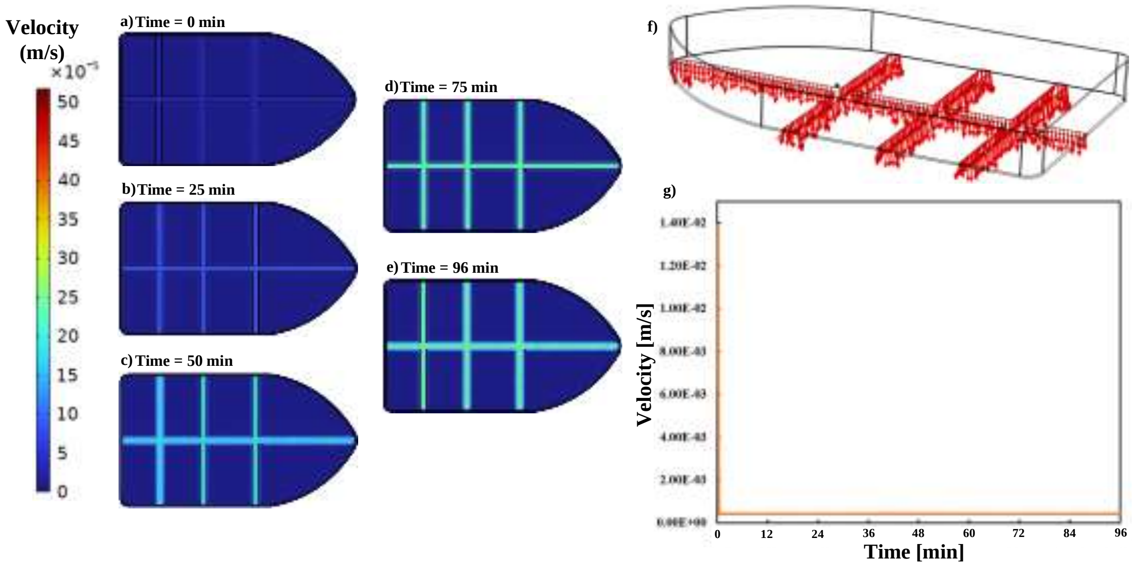

Figure 17. a-e) Velocity contours, f) streamlines, and g) variations for the fishbone strategy at different time intervals.

The streamlines from both strategies offer crucial insights into the resin flow dynamics during injection. For the cylindrical inlet strategy, the observed streamlines hint at a gradual decline in the resin flow velocity, suggesting potential variations in the resin distribution within the mold cavity during the injection process. The velocity profile along the small vessel hull (Figure 16b) showcases a declining trend from an initial velocity of 1×10^{-3} m/s to a steady-state of 1×10^{-6} m/s, indicating a controlled and gradual resin infiltration. Contrastingly, the streamlines for the fishbone strategy indicate higher initial resin velocities compared to the cylindrical strategy, potentially implying a quicker and more extensive resin infusion into the mold. The velocity contours in Figure 17a-e portray consistent resin flow patterns over time, suggesting a more uniform resin distribution within the mold compared to the gradual and controlled flow observed in the cylindrical strategy. In Figure 17g, at 0 min, the resin velocity initiates at roughly 1.4×10^{-2} m/s and eventually stabilizes at 1×10^{-6} m/s. Understanding these flow dynamics holds significance for optimizing resin injection techniques in small vessel hull fabrication. The distinct behaviors observed in the resin flow between the cylindrical and fishbone strategies provide valuable insights into the efficiency and uniformity of the resin distribution within the mold. These insights are pivotal for ensuring the structural integrity and quality of the manufactured vessels.

Similar to the pressure analysis, detailed velocity contour distributions are presented only for the cylindrical and fishbone configurations because these two injection layouts effectively illustrate the two representative flow behaviors identified in this study. The cylindrical configuration exhibits relatively localized high-velocity regions accompanied by less uniform flow development, whereas the fishbone configuration produces a more homogeneous velocity field and smoother resin advancement throughout the mold cavity. The radial, parallel, and alternating configurations displayed intermediate velocity characteristics that followed the same overall flow trends and were already quantitatively evaluated through the filling time, resin flow evolution, and impregnation analyses. Consequently, presenting velocity contour plots for all investigated configurations would mainly introduce redundant information without substantially improving the physical interpretation of the results.

5. Conclusion

This study presented a comprehensive numerical investigation of the resin infusion behavior during the manufacturing of composite small-vessel hulls using a three-dimensional two-phase Level-Set formulation. Five resin injection configurations, namely Cylindrical, Fishbone, Radial, Parallel, and Alternating arrangements, were systematically evaluated to investigate their influence on the resin flow evolution, filling time, pressure distribution, velocity characteristics, gelation behavior, impregnation quality, and potential susceptibility to incomplete saturation. The results confirmed that the selection of the injection strategy plays a decisive role in determining both the manufacturing efficiency and the overall quality of the resin infusion process. The numerical simulations revealed that the investigated injection configurations exhibit different advantages depending on the selected performance criterion. The Alternating configuration achieved the shortest mold filling time, demonstrating the highest production efficiency among all investigated layouts. In contrast, the Fishbone configuration provided the most uniform resin distribution, smoother pressure gradients, more homogeneous velocity fields, and improved impregnation characteristics throughout the mold cavity. The Radial configuration exhibited balanced filling behavior and acceptable impregnation quality, while the Cylindrical and Parallel arrangements showed relatively slower filling behavior and a greater qualitative tendency toward localized incomplete saturation. Therefore, the present results indicate that no single injection strategy is universally superior for every manufacturing objective; instead, the optimal configuration depends on the specific performance requirements of the manufacturing process.

To facilitate engineering interpretation of the numerical results, the overall performance of the investigated injection strategies is summarized in Table 5. The comparison clearly demonstrates that although the Alternating configuration is preferable when minimizing the mold filling time is the primary objective, the Fishbone configuration provides the most balanced overall engineering performance by simultaneously improving the resin distribution uniformity, flow stability, impregnation quality, and manufacturing reliability. Consequently, the Fishbone arrangement is recommended for applications where overall manufacturing quality and process robustness are considered more important than achieving the absolute minimum filling time.

Table 5.
Overall engineering performance assessment of the investigated resin injection configurations

Performance Criterion	Best Configuration
Shortest mold filling time	Alternating
Most uniform resin distribution	Fishbone
Most homogeneous pressure distribution	Fishbone
Most stable velocity field	Fishbone
Lowest qualitative risk of incomplete impregnation	Fishbone / Alternating
Best overall engineering performance	Fishbone

The comparative assessment presented in Table 5 highlights that the selection of an appropriate injection strategy should not rely solely on the mold filling time. Although production efficiency is an important design criterion, manufacturing quality is also governed by the resin distribution uniformity, flow stability, pressure evolution, and ability to minimize incomplete impregnation. Considering all these performance indicators simultaneously, the Fishbone configuration exhibits the most balanced behavior among the investigated layouts and therefore represents the preferred engineering solution for manufacturing composite small-vessel hulls. Beyond the specific numerical findings, this study provides practical engineering guidance for selecting appropriate resin injection layouts during the design of composite marine structures. The proposed numerical methodology can substantially reduce the dependence on costly trial-and-error procedures during mold development while supporting more efficient process planning and optimization.

Despite these contributions, several limitations should be acknowledged. The present investigation was limited to the numerical simulations performed under predefined processing conditions, and the experimental validation was introduced through comparison with the published experimentally validated literature rather than dedicated laboratory experiments for all investigated injection configurations. Furthermore, the numerical model assumes constant resin viscosity throughout the filling process and does not explicitly account for the curing kinetics, temperature-dependent material properties, microscale resin–fiber interactions, or direct prediction of the void nucleation and growth. The assessment of the potential air entrapment presented in this study is therefore qualitative and inferred from the predicted resin flow characteristics rather than the direct simulation of multiphase air–resin interactions. Future research should focus on the comprehensive experimental validation of the investigated injection strategies, incorporation of coupled thermo-fluid curing models with temperature-dependent resin viscosity, implementation of advanced permeability and air–resin interaction models for quantitative void prediction, and optimization of process parameters using machine learning and artificial intelligence techniques. Moreover, establishing quantitative correlations between the resin flow behavior, impregnation quality, and the structural and mechanical performance of manufactured composite hulls would further improve the predictive capability and industrial applicability of numerical resin infusion simulations.

Acknowledgements

This research did not receive any specific grant from funding agencies in the public, commercial, or not-for-profit sectors.

CrediT authorship contribution statement

Saeed Ghasemzade Bariki: Methodology, Formal analysis, Software, Validation, Resources, Investigation, Writing original draft. **Mehrdad Mahmoudi:** Conceptualization, Methodology, Software, Writing – review & editing. **Salman Movahedirad:** Supervision, Project administration.

Competing Interests

The authors declare that they have no known competing financial interests or personal relationships that could have appeared to influence the work reported in this paper.

Data availability statement

The datasets generated and/or analyzed during the current study are available from the corresponding author on reasonable request.

References

[1] Arora H, Kelly M, Worley A, Del Linz P, Fergusson A, Hooper P, Dear J (2014) Compressive strength after blast of sandwich composite materials. Philosophical Transactions of the Royal Society A: Mathematical, Physical and Engineering Sciences 372: 20130212. DOI: 10.1098/rsta.2013.0212.

[2] Lee H, Jung K, Park H (2021) Study on structural design and analysis of composite boat hull manufactured by resin infusion simulation. Materials 14: 5918. DOI: 10.3390/ma14205918.

[3] Verma KK, Dinesh B, Singh K, Gaddikeri KM, Sundaram R (2014) Challenges in processing of a cocured wing test box using vacuum enhanced resin infusion technology (VERITy). Procedia Materials Science 6: 331-340. DOI: 10.1016/j.mspro.2014.07.042.

[4] Teixeira TA, Souza JA (2019) Computational modeling of resin infusion process applied to small vessel hulls. Journal of the Brazilian Society of Mechanical Sciences and Engineering 41: 1-9. DOI: 10.1007/s40430-019-1936-z.

[5] Mathijsen D (2016) Now is the time to make the change from metal to composites in naval shipbuilding. Reinforced Plastics 60: 289-293.

[6] Gromada M, Świeca A, Kostecki M, Olszyna A, Cygan R (2015) Ceramic cores for turbine blades via injection moulding. Journal of Materials Processing Technology 220: 107-112. DOI: 10.1016/j.jmatprotec.2015.01.010.

[7] Michaud V (2016) A review of non-saturated resin flow in liquid composite moulding processes. Transport in Porous Media 115: 581-601. DOI: 10.1007/s11242-016-0629-7.

[8] Ageyeva T, Sibikin I, Kovács JG (2019) A review of thermoplastic resin transfer molding: Process modeling and simulation. Polymers 11: 1555. DOI: 10.3390/polym11101555.

[9] Agwa M, Youssef SM, Ali-Eldin SS, Megahed M (2022) Integrated vacuum assisted resin infusion and resin transfer molding technique for manufacturing of nano-filled glass fiber reinforced epoxy composite. Journal of Industrial Textiles 51: 5113S-5144S. DOI: 10.1177/1528083720932337.

[10] Bodaghi M, Costa R, Gomes R, Silva J, Correia N, Silva F (2020) Experimental comparative study of the variants of high-temperature vacuum-assisted resin transfer moulding. Elsevier 105708. DOI: 10.1016/j.compositesa.2019.105708.

[11] Delucis RDA, Tonatto MLP, Trindade RS, Amico SC (2021) In situ L-RTM manufacturing of sandwich panels with PET foam core reinforced by polymeric pins. Journal of Sandwich Structures & Materials 23: 241-254. DOI: 10.1177/1099636219830145.

[12] Vita A, Castorani V, Germani M, Marconi M (2019) Comparative life cycle assessment of low-pressure RTM, compression RTM and high-pressure RTM manufacturing processes to produce CFRP car hoods. Procedia CIRP 80: 352-357. DOI: 10.1016/j.procir.2019.01.109.

[13] Govignon Q, Bickerton S, Kelly P (2023) Liquid composite molding processes. In: Advanced Fiber-Reinforced Polymer (FRP) Composites for Structural Applications. Elsevier, pp. 101-136.

[14] Hassan MH (2021) A mini review on manufacturing defects and performance assessments of complex shape prepreg-based composites. The International Journal of Advanced Manufacturing Technology 115: 3393-3408. DOI: 10.1007/s00170-021-07421-8.

[15] Bo Y, Shilong W, Qian T (2019) Modeling and 3D simulation of the mould compression and resin flow for force-controlled compression resin transfer moulding. Materials Science (Medžiagotyra) 25. DOI: 10.5755/j01.ms.25.1.19134.

[16] Härter FV, Souza JA, Isoldi LA, Santos EDD, Amico SC (2017) Transverse permeability determination and influence in resin flow through an orthotropic medium in the RTM process. Matéria (Rio de Janeiro) 22: e11851. DOI: 10.1590/s1517-707620170002.0167.

[17] Magagnato D, Seuffert J, Bernath A, Kärger L, Henning F (2018) Experimental and numerical study of the influence of integrated load transmission elements on filling behavior in resin transfer molding. Composite Structures 198: 135-143. DOI: 10.1016/j.compstruct.2018.05.021.

[18] Yang W, Lu S, Xiang L, Liu W (2019) Nonisothermal simulation on pressure during resin transfer molding. Journal of Applied Polymer Science 136: 47492. DOI: 10.1002/app.47492.

[19] Koutsonas S (2018) Modelling race-tracking variability of resin rich zones on 90 composite 2.2 twill fibre curved plate. Composites Science and Technology 168: 448-459. DOI: 10.1016/j.compscitech.2018.08.001.

[20] Mustafa I (1998) A 3-D nonisothermal flow simulation and pulling force model for injection pultrusion processes. Washington University in St. Louis.

[21] Souza JA, Rocha LAO, Amico SC, Vargas JVC (2011) A numerical investigation of the resin flow front tracking applied to the RTM process. Materials Research 14: 345-354. DOI: 10.1590/S1516-14392011005000049.

[22] Rubino F (2018) Analysis and enhancement of resin flow in liquid composite molding process. http://elea.unisa.it/xmlui/handle/10556/3035.

[23] Torrent RJ, Neves RD, Imamoto K-I (2021) Concrete permeability and durability performance: From theory to field applications. CRC Press. DOI: 10.1201/9780429505652.

[24] Isoldi LA, Oliveira CP, Rocha LA, Souza JA, Amico SC (2012) Three-dimensional numerical modeling of RTM and LRTM processes. Journal of the Brazilian Society of Mechanical Sciences and Engineering 34: 105-111. DOI: 10.1590/S1678-58782012000200001.

[25] Joubaud L, Achim V, Trochu F (2005) Numerical simulation of resin infusion and reinforcement consolidation under flexible cover. Polymer Composites 26: 417-427. DOI: 10.1002/pc.20069.

[26] Correia N, Robitaille F, Long A, Rudd C, Šimáček P, Advani S (2005) Analysis of the vacuum infusion moulding process: I. Analytical formulation. Composites Part A: Applied Science and Manufacturing 36: 1645-1656. DOI: 10.1016/j.compositesa.2005.03.019.

[27] Trochu F, Ruiz E, Achim V, Soukane S (2006) Advanced numerical simulation of liquid composite molding for process analysis and optimization. Composites Part A: Applied Science and Manufacturing 37: 890-902. DOI: 10.1016/j.compositesa.2005.06.003.

[28] Govignon Q, Bickerton S, Kelly P (2010) Simulation of the reinforcement compaction and resin flow during the complete resin infusion process. Composites Part A: Applied Science and Manufacturing 41: 45-57. DOI: 10.1016/j.compositesa.2009.07.007.

[29] Adhikari D, Gururaja S, Hemchandra S (2021) Vacuum infusion in porous preform with different mould configurations: Flow

simulation and experimental validation. Journal of Reinforced Plastics and Composites 40: 321-338. DOI: 10.1177/0731684420960209.

[30] Adhikari D, Gururaja S, Hemchandra S, Kočí J (2023) Resin infusion in porous preform in the presence of HPM considering complex geometry and gravity: Flow simulation and experimental validation. Journal of Reinforced Plastics and Composites 42: 971-989. DOI: 10.1177/07316844221143517.

[31] Li C, Huang J, Qin T, Chen C, Gao L, Xu J (2022) A novel approach to simulate the resin infusion process by two phases coupling free and porous flows intra and inter fiber tows of liquid composite molding. Journal of Composite Materials 56: 3359-3367. DOI: 10.1177/00219983221111495.

[32] do Nascimento Santos M, Delgado JM, Barbosa de Lima A, Rodrigues I (2019) Resin flow in porous-fibrous media: An application to polymer composite manufacturing. Diffusion Foundations 20: 1-15. DOI: 10.4028/www.scientific.net/df.20.1.

[33] Sandberg M, Yuksel O, Baran I, Hattel JH, Spangenberg J (2021) Numerical and experimental analysis of resin-flow, heat-transfer, and cure in a resin-injection pultrusion process. Composites Part A: Applied Science and Manufacturing 143: 106231. DOI: 10.1016/j.compositesa.2020.106231.

[34] Lu JG, Lee SB, Lundström TS, Hwang WR (2022) Numerical simulation on void formation and migration using Stokes-Brinkman coupling with effective dual-scale fibrous porous media. Composites Part A: Applied Science and Manufacturing 152: 106683. DOI: 10.1016/j.compositesa.2021.106683.

[35] Mirjalili S, Ivey CB, Mani A (2020) A conservative diffuse interface method for two-phase flows with provable boundedness properties. Journal of Computational Physics 401: 109006. DOI: 10.1016/j.jcp.2019.109006.

[36] Bariki SG, Movahedirad S (2022) A flow map for core/shell microdroplet formation in the co-flow microchannel using ternary phase-field numerical model. Scientific Reports 12: 22010. DOI: 10.1038/s41598-022-26648-3.

[37] Ghasemzade Bariki S, Movahedirad S (2024) Hydrodynamic characteristics of core/shell microdroplets formation: map of the flow patterns in double-T microchannel. Chemical Engineering Journal, 479, p.147749. DOI: 10.1016/j.cej.2023.147749.

[38] Ghasemzade Bariki S, Salman M, Movahedirad S (2023) Computational fluid dynamic study of polycaprolactone nanoparticles precipitation in a co-flow capillary micro-tube. The Canadian Journal of Chemical Engineering 101: 4746-4761. DOI:10.1002/cjce.24768

[39] Mahmoudi M, Ghasemzade Bariki S, Movahedirad S (2024) Comprehensive analysis and CFD modeling of slug and detachment length in the T-junction micro-channel using RSM. Iranian journal of chemistry and chemical engineering 43: 4089-4099. DOI: 10.30492/ijcce.2024.2026580.6542.

[40] Vilà J, González C, Llorca J (2014) A level set approach for the analysis of flow and compaction during resin infusion in composite materials. Composites Part A: Applied Science and Manufacturing 67: 299-307. DOI: 10.1016/j.compositesa.2014.09.002.